Datasheet for 600-401-914

Histone H2AvD phosphoS137 Antibody

Overview

Description:	Anti-Histone H2AvD pS137 (RABBIT) Antibody - 600-401-914
Item No.:	600-401-914
Size:	100 µg
Applications:	ELISA, IHC, WB, ChIP, EM, IF, Multiplex
Reactivity:	D. melanogaster
Host Species:	Rabbit

Product Details

Background:	This antibody is designed, produced, and validated as part of a collaboration between Rockland and the National Cancer Institute (NCI) and is suitable for Cancer, Immunology and Nuclear Signaling research. Variant histones H2A are synthesized throughout the cell cycle and are very different from classical S-phase regulated H2A. H2AvD is vital for viability, but the exact function of variant histones H2A is not known. H2A is a core component of the nucleosome, an octamer containing two molecules each of H2A, H2B, H3 and H4. The octamer wraps approximately 146 bp of DNA. HsAvD is expressed both maternally and zygotically and is found in embryos through to adults (female only). The human homologue, H2AX, is phosphorylated by ATM protein kinase when double strand DNA breaks occur. In mouse, H2AX ''knock out'' mice have an increased incidence of cancer.
Synonyms:	rabbit anti-H2AvD pS137 antibody, rabbit anti-Histone H2A.v pS137 antibody, H2AvD protein antibody, H2A.F/Z, H2A.Z, H2AvD, His2AvD, His2Av
Host Species:	Rabbit
Clonality:	Polyclonal
Format:	IgG

Target Details

Gene Name:	His2Av
Reactivity:	D. melanogaster
PTM Specificity:	Phosphorylation

Immunogen Type:	Conjugated Peptide
Immunogen:	Histone H2AvD pS137 Antibody was prepared from whole rabbit serum produced by repeated immunizations with a synthetic peptide corresponding to the C-Terminal region near amino acids 125-141 of Drosophila melanogaster (fruit fly) H2AvD protein.
Purity/Specificity:	Affinity purified Anti-Histone H2AvD pS137 Antibody is directed against the phosphorylated form of Drosophila H2AvD protein at the pS137 residue. The product was affinity purified from monospecific antiserum by immunoaffinity purification. Antiserum was first purified against the phosphorylated form of the immunizing peptide. The resultant affinity purified antibody was then cross-adsorbed against the non-phosphorylated form of the immunizing peptide. Reactivity occurs against Drosophila H2AvD pS137 protein and the antibody is specific for the phosphorylated form of the protein. Reactivity with non-phosphorylated Drosophila H2AvD is minimal by ELISA. A BLAST analysis was used to suggest little to no cross reactivity with H2AvD proteins from other sources based on a comparison using the immunizing sequence. Reactivity against homologues from other sources is not known.
Relevant Links:	• UniProtKB - P08985 • NCBI - 17738227 • GeneID - 43229

Application Details

Tested Applications:	ELISA, IHC, WB
Suggested Applications:	ChIP, EM, IF, Multiplex (Based on references)
Application Note:	Histone H2AvD pS137 Antibody is tested in ELISA, Immunohistochemistry, and by western blot. Specific conditions for reactivity should be optimized by the end user. Expect a band approximately 14 kDa in size corresponding to phosphorylated H2AvD protein by western blotting in the appropriate Drosophila tissue or cell lysate or extract. Minimal reactivity is observed against the non-phosphorylated form of the immunizing peptide. This antibody is phospho specific for pS137 of H2AvD protein.
Assay Dilutions:	All assays should be optimized by the user. Recommended dilutions (if any) may be listed below.
ELISA:	1:29,000 - 1:30,000
IHC:	2 ug/ml
WB:	1:400 - 1:1,600

Formulation

Physical State:	Liquid (sterile filtered)

Concentration:	1.01 mg/mL by UV absorbance at 280 nm
Buffer:	0.02 M Potassium Phosphate, 0.15 M Sodium Chloride, pH 7.2
Preservative:	0.01% (w/v) Sodium Azide
Stabilizer:	None

Shipping & Handling

Shipping Condition:	Dry Ice
Storage Condition:	Store vial at -20° C prior to opening. Aliquot contents and freeze at -20° C or below for extended storage. Avoid cycles of freezing and thawing. Centrifuge product if not completely clear after standing at room temperature. This product is stable for several weeks at 4° C as an undiluted liquid. Dilute only prior to immediate use.
Expiration:	Expiration date is one (1) year from date of receipt.

Images

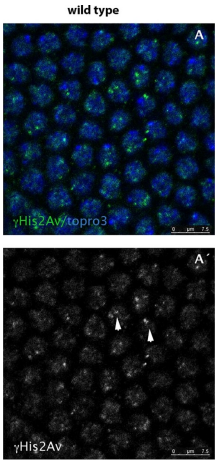

Immunofluorescence Microscopy
hth mutant nuclei show increased number of DNA breaks.A,A´) Wild type syncytium (cycle 11) stained for His2AvP (green) and topro3 (blue). Due to the lack of mitotic checkpoints during the rapid syncytial divisions the nuclei show some degree of DNA breaks marked with the anti-His2AvP antibody (arrowheads in A´). B, B´) However, hth mutant nuclei show more nuclear signal when stained with the same antibody (see arrows in B´) indicating that they have more breaks in their DNA. C) Quantification of the DNA breaks in the Dfhth mutant embryos and in their wild type siblings. Quantification was performed by counting the number of nuclear dots marked with the anti-His2AvP antibody. (N = 50 nuclei for each genotype from 5 different embryos each. P-value: 7,0085X10−5). Figure provided by CiteAb. Source: PLoS One, PMID: 25794008.

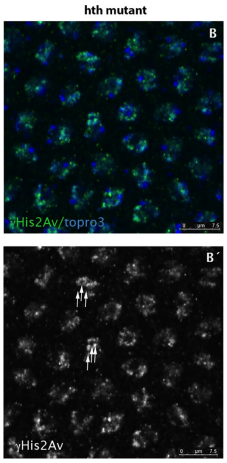

Immunofluorescence Microscopy
hth mutant nuclei show increased number of DNA breaks.A,A´) Wild type syncytium (cycle 11) stained for His2AvP (green) and topro3 (blue). Due to the lack of mitotic checkpoints during the rapid syncytial divisions the nuclei show some degree of DNA breaks marked with the anti-His2AvP antibody (arrowheads in A´). B, B´) However, hth mutant nuclei show more nuclear signal when stained with the same antibody (see arrows in B´) indicating that they have more breaks in their DNA. C) Quantification of the DNA breaks in the Dfhth mutant embryos and in their wild type siblings. Quantification was performed by counting the number of nuclear dots marked with the anti-His2AvP antibody. (N = 50 nuclei for each genotype from 5 different embryos each. P-value: 7,0085X10−5). Figure provided by CiteAb. Source: PLoS One, PMID: 25794008.

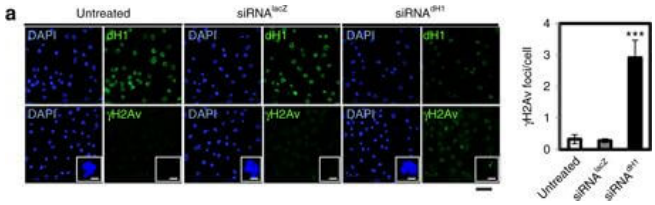

Immunocytochemistry

dH1 depletion induces DNA damage. a Immunostaining of dH1-depleted (siRNAdH1) and control undepleted cells (siRNAlacZ and untreated) with αdH1 and αγH2Av antibodies (both in green). DNA was stained with DAPI (blue). Insets show enlarged images of representative individual cells. Scale bars are 20 µm and 2 µm in the Insets. On the right, the number of γH2Av foci per cell is presented (n > 100 for each condition). Error bars are s.e.m. The p-value of siRNAdH1 respect to siRNAlacZ is indicated (***p<0.005; two-tailed Student's t-test). b WB analyses with αdH1, αγH2Av and αH4 of increasing amounts of extracts (lanes 1–3) prepared from siRNAdH1, siRNAlacZ and untreated cells. The positions corresponding to molecular weight markers are indicated. On the right, quantitative analysis of the results (N = 3). Error bars are s.e.m. The p-value of siRNAdH1 respect to siRNAlacZ is indicated (***<0.005; two-tailed Student's t-test). c Alkaline and neutral single-cell electrophoresis analyses of siRNAdH1, siRNAlacZ and untreated cells. Scale bar corresponds to 20 µm. On the right, relative comet-tail moments are presented (n > 100 for each condition). Error bars are s.e.m. The p-values of siRNAdH1 respect to siRNAlacZ are indicated (***<0.005; two-tailed Student's t-test). d On the top, WB analysis with αγH2Av and αtubulin at different time points after X-ray irradiation (10 Gy) of siRNAdH1 and untreated cells. The positions corresponding to molecular weight markers are indicated. On the bottom, quantitative analysis of the results (N = 3) Figure provided by CiteAb. Source: Nat Commun, PMID: 28819201.

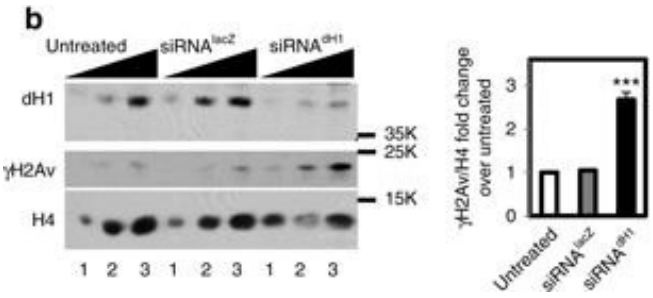

Western Blot

dH1 depletion induces DNA damage. a Immunostaining of dH1-depleted (siRNAdH1) and control undepleted cells (siRNAlacZ and untreated) with αdH1 and αγH2Av antibodies (both in green). DNA was stained with DAPI (blue). Insets show enlarged images of representative individual cells. Scale bars are 20 µm and 2 µm in the Insets. On the right, the number of γH2Av foci per cell is presented (n > 100 for each condition). Error bars are s.e.m. The p-value of siRNAdH1 respect to siRNAlacZ is indicated (***p<0.005; two-tailed Student's t-test). b WB analyses with αdH1, αγH2Av and αH4 of increasing amounts of extracts (lanes 1–3) prepared from siRNAdH1, siRNAlacZ and untreated cells. The positions corresponding to molecular weight markers are indicated. On the right, quantitative analysis of the results (N = 3). Error bars are s.e.m. The p-value of siRNAdH1 respect to siRNAlacZ is indicated (***<0.005; two-tailed Student's t-test). c Alkaline and neutral single-cell electrophoresis analyses of siRNAdH1, siRNAlacZ and untreated cells. Scale bar corresponds to 20 µm. On the right, relative comet-tail moments are presented (n > 100 for each condition). Error bars are s.e.m. The p-values of siRNAdH1 respect to siRNAlacZ are indicated (***<0.005; two-tailed Student's t-test). d On the top, WB analysis with αγH2Av and αtubulin at different time points after X-ray irradiation (10 Gy) of siRNAdH1 and untreated cells. The positions corresponding to molecular weight markers are indicated. On the bottom, quantitative analysis of the results (N = 3) Figure provided by CiteAb. Source: Nat Commun, PMID: 28819201.

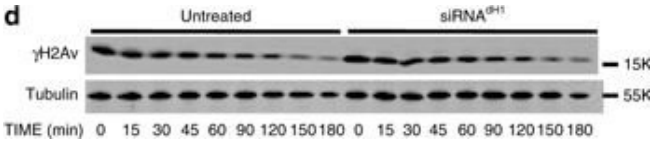

Western Blot

dH1 depletion induces DNA damage. a Immunostaining of dH1-depleted (siRNAdH1) and control undepleted cells (siRNAlacZ and untreated) with αdH1 and αγH2Av antibodies (both in green). DNA was stained with DAPI (blue). Insets show enlarged images of representative individual cells. Scale bars are 20 µm and 2 µm in the Insets. On the right, the number of γH2Av foci per cell is presented (n > 100 for each condition). Error bars are s.e.m. The p-value of siRNAdH1 respect to siRNAlacZ is indicated (***p<0.005; two-tailed Student's t-test). b WB analyses with αdH1, αγH2Av and αH4 of increasing amounts of extracts (lanes 1–3) prepared from siRNAdH1, siRNAlacZ and untreated cells. The positions corresponding to molecular weight markers are indicated. On the right, quantitative analysis of the results (N = 3). Error bars are s.e.m. The p-value of siRNAdH1 respect to siRNAlacZ is indicated (***<0.005; two-tailed Student's t-test). c Alkaline and neutral single-cell electrophoresis analyses of siRNAdH1, siRNAlacZ and untreated cells. Scale bar corresponds to 20 µm. On the right, relative comet-tail moments are presented (n > 100 for each condition). Error bars are s.e.m. The p-values of siRNAdH1 respect to siRNAlacZ are indicated (***<0.005; two-tailed Student's t-test). d On the top, WB analysis with αγH2Av and αtubulin at different time points after X-ray irradiation (10 Gy) of siRNAdH1 and untreated cells. The positions corresponding to molecular weight markers are indicated. On the bottom, quantitative analysis of the results (N = 3) Figure provided by CiteAb. Source: Nat Commun, PMID: 28819201.

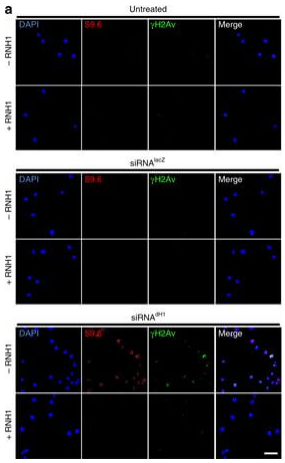

Immunocytochemistry

DNA damage induced by dH1 depletion associates with R-loops accumulation. a Immunostainings with αγH2Av (green) and S9.6 (red) antibodies of siRNAdH1, siRNAlacZ and untreated cells overexpressing human RNH1 (+) or not (−). Scale bar corresponds to 10 µm. b Quantitative analysis of the results shown in a. S9.6 (top) and γH2Av (center) reactivities determined as the proportion of DAPI area stained with S9.6 antibodies and the number of γH2Av foci per cell are presented (n > 50 for each condition). On the bottom, the extent of γH2Av/S9.6 colocalization is presented as the proportion of γH2Av area overlapping with S9.6 reactivity (n > 50 for each condition). Error bars are s.e.m. The p-values of siRNAdH1 respect to siRNAlacZ are indicated (no asterisk >0.05, ***<0.005; two-tailed Student's t-test). c αγH2Av (top) and S9.6 (bottom) reactivities of G1-, S- and G2/M-phase sorted siRNAdH1, siRNAlacZ and untreated cells overexpressing RNH1 (+) or not (−) are presented as in b (n > 50 for each condition). Error bars are s.e.m. The p-values of siRNAdH1 respect to siRNAlacZ are indicated (no asterisk >0.05, ***<0.005; two-tailed Student's t-test). d WB analyses with αdH1, αγH2Av and αH4 antibodies of siRNAdH1 and untreated cells sorted at G1-, S and G2/M-phase. The positions corresponding to molecular weight markers are indicated. Quantitative analysis is shown on the bottom (N = 2). Error bars are s.e.m. The p-values respect to untreated are indicated (no asterisk >0.05, **<0.01, ***<0.005; two-tailed Student's t-test) Figure provided by CiteAb. Source: Nat Commun, PMID: 28819201.

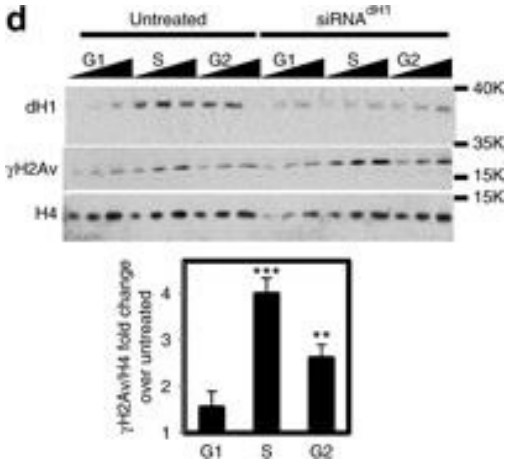

Western Blot

DNA damage induced by dH1 depletion associates with R-loops accumulation. a Immunostainings with αγH2Av (green) and S9.6 (red) antibodies of siRNAdH1, siRNAlacZ and untreated cells overexpressing human RNH1 (+) or not (−). Scale bar corresponds to 10 µm. b Quantitative analysis of the results shown in a. S9.6 (top) and γH2Av (center) reactivities determined as the proportion of DAPI area stained with S9.6 antibodies and the number of γH2Av foci per cell are presented (n > 50 for each condition). On the bottom, the extent of γH2Av/S9.6 colocalization is presented as the proportion of γH2Av area overlapping with S9.6 reactivity (n > 50 for each condition). Error bars are s.e.m. The p-values of siRNAdH1 respect to siRNAlacZ are indicated (no asterisk >0.05, ***<0.005; two-tailed Student's t-test). c αγH2Av (top) and S9.6 (bottom) reactivities of G1-, S- and G2/M-phase sorted siRNAdH1, siRNAlacZ and untreated cells overexpressing RNH1 (+) or not (−) are presented as in b (n > 50 for each condition). Error bars are s.e.m. The p-values of siRNAdH1 respect to siRNAlacZ are indicated (no asterisk >0.05, ***<0.005; two-tailed Student's t-test). d WB analyses with αdH1, αγH2Av and αH4 antibodies of siRNAdH1 and untreated cells sorted at G1-, S and G2/M-phase. The positions corresponding to molecular weight markers are indicated. Quantitative analysis is shown on the bottom (N = 2). Error bars are s.e.m. The p-values respect to untreated are indicated (no asterisk >0.05, **<0.01, ***<0.005; two-tailed Student's t-test) Figure provided by CiteAb. Source: Nat Commun, PMID: 28819201.

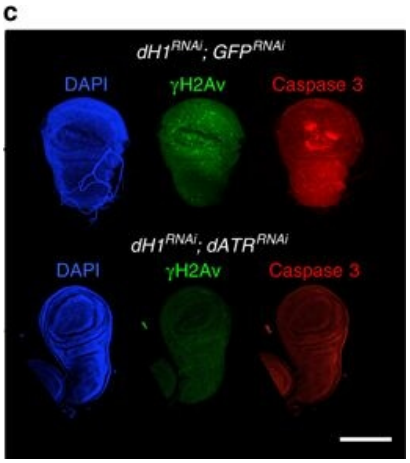

Western Blot

R-loops induced by dH1 depletion activate JNK-dependent apoptosis. a Wings from dH1-depleted his1RNAi flies of the indicated genotypes where dH1 depletion was induced in the pouch region of the wing imaginal disc. Scale bar corresponds to 500 µm. b Quantitative analysis of the wing area of dH1-depleted his1RNAi flies of the indicated genotypes. Data is expressed as fold change respect to control dH1-depleted his1RNAi; GFPRNAi (n > 20 for each condition). Error bars are s.e.m. The p-values respect to control his1RNAi; GFPRNAi are indicated (**<0.01, ***<0.005; two-tailed Student's t-test). c Immunostaining with αγH2Av (green) and αCaspase 3 (red) of wing imaginal discs from dH1-depleted his1RNAi flies upon dATRRNAi co-depletion (bottom) or not (top). DNA was stained with DAPI (blue). d Immunostaining with αCaspase 3 (red) of wing imaginal discs from dH1-depleted his1RNAi flies upon p53RNAi co-depletion (bottom) or p53H159N overexpression (top). DNA was stained with DAPI (blue). e As in d but upon bskRNAi co-depletion (top) or puc2A overexpression (bottom). Scale bars in c–e are 200 µm
Figure provided by CiteAb. Source: Nat Commun, PMID: 28819201.

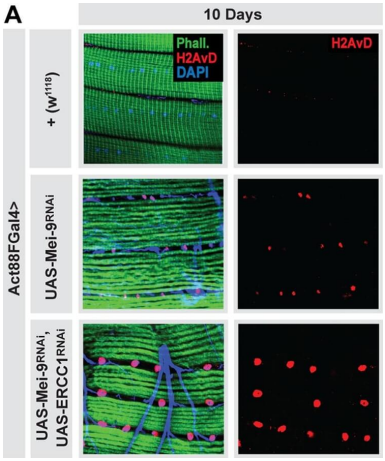

Immunofluorescence Microscopy

Systemic hormetic responses from muscle-specific DNA damage.(A) Detection of DNA damage (double strand breaks) in dissected longitudinal thoracic muscle of young (10 d) Act88FG4>+(w1118) controls, and flies with DNA repair attenuation specifically in thoracic muscle (mu-specific, Act88FG4>UAS-Mei-9RNAi or Act88FG4>UAS-Mei-9RNAi, UAS-ERCC1RNAi); assayed by phospho-H2aV immunostaining (red), counterstained with phalloidin ("Phall"; green, actin filaments) and DAPI (blue). Representative images shown. (B) Immunostaining to detect poly-ubiquitin protein (aggregates; "Poly-Ub.") in dissected longitudinal thoracic muscle from young (10 d) and old (30 d) flies, genotypes described above; anti-poly-ubiquitin (green), counterstained with phalloidin (red, actin filaments). Representative images shown. (C-D). Survival curves (lifespan, female flies) associated with mu-specific inhibition of Mei-9 using (C) the Act88FGal4 driver (compared to Act88FG4>+[w1118] controls) or (D) a GeneSwitch inducible driver (Act88FGS, +RU486 compared with −RU486 [vehicle alone] sibling controls). (E) Quantification of mitoses per whole dissected midgut

(assayed by anti-pH3 immunostaining) at indicted ages, genotypes described above; bars represent mean ± SE, n = 25–30. (F) Immunostaining of dissected intestines to assess epithelial integrity of posterior midguts at indicated ages, genotypes described above; pH3 (green), armadillo ("Arm"; membrane, red), and DAPI (blue). Representative images shown. (G-H) Lineage tracing from ISCs using FRT recombination of a split alpha-tubulin-lacZ transgene (in Act88FG4>+[w1118, controls] or Act88FG4>UAS-Mei-9RNAi genetic background). (G) Changes in clone size (cell per clone form posterior midgut) at indicated ages; represented as box plot (median, red line), n = 25. (H) Representative images of lacZ clones from various genotypes at indicated ages, immunostaining of dissected midguts (posterior), anti-lacZ (green), and DAPI (blue). (I) Venn diagrams showing overlap of up-regulated genes (from dissected midguts) between Act88FG4>UAS-Mei-9RNAi and controls Act88FGal4> +(w1118) during aging (transcriptomes at 30 d, compared to Act88FGal4>+[w1118] controls at day 10). The threshold for genes included in the analysis was (i) changes in RPKM values of at least 2-fold up-regulated in intestine compared to young controls and (ii) a minimum RPKM value of 2. (J) Fold change (in intestinal transcriptome RPKM values; Day 30 Act88FG4>UAS-Mei-9RNAi/ Day 10 Act88FGal4>+[w1118] control [black bars] or Day 30 control/Day 10 control [gray bars]) of selected innate immune genes. Underlying data can be found in S1 Data. See also S1 and S2 Figs and S1 and S2 Tables. FRT, flippase recombination target; ISC, intestinal stem cell; pH3, phospho Histone H3; mu-specific, muscle-specific; RPKM, reads per kbp per million reads; RU486, mifepristone. Figure provided by CiteAb. Source: PLoS Biol, PMID: 30036358.

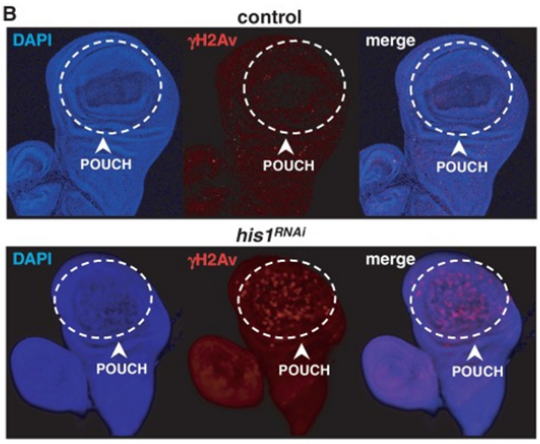

Immunofluorescence Microscopy
(B) γH2Av levels were determined by immunostaining using αγH2Av antibodies (1:1000; red) in wing imaginal discs prepared from mutant his1RNAi; nub-GAL4; UASGAL4-Dcr2 and control GFPRNAi; nub-GAL4; UASGAL4-Dcr2 larvae. The region corresponding to the pouch is indicated. DNA was stained with DAPI. Fig 4. PMID: 22406835

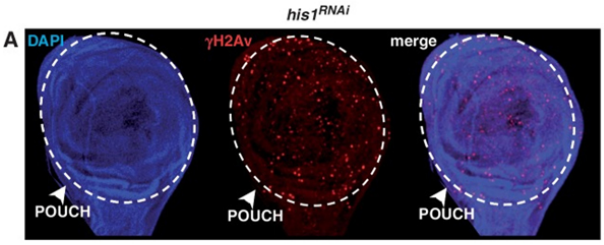

Immunofluorescence Microscopy
Blocking apoptosis by p35 over-expression rescues proliferation of dH1-depleted cells. (A) γH2Av levels were determined by immunostaining using αγH2Av antibodies (1:1000; red) in wing imaginal discs prepared from mutant his1RNAi; nub-GAL4; UASGAL4-Dcr2; UASGAL4-p35. The region corresponding to the pouch is indicated. DNA was stained with DAPI. Fig 6. PMID: 22406835

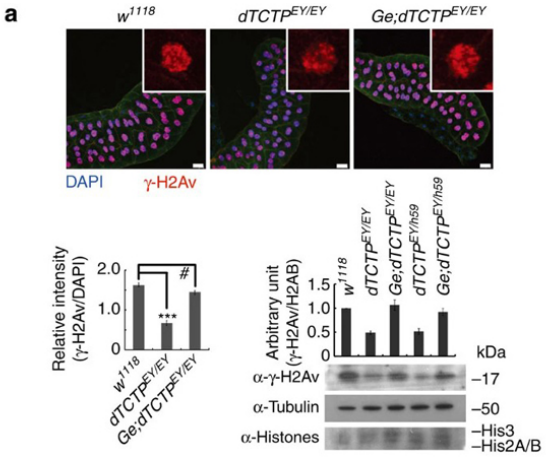

Immunofluorescence Microscopy

a) Reduction of nuclear γ-H2Av level (red) in third instar larval salivary gland of dTCTP mutants. (Upper left) endocycling salivary gland cells have many DSBs in their nuclei (insets, γ-H2Av stained cell nuclei in a higher magnification). (Upper middle) reduced γ-H2Av level in homozygous dTCTPEY09182 mutant (dTCTPEY/EY). (Upper right) dTCTPEY/EY mutants are rescued by the genomic dTCTPGe transgene (Ge;dTCTPEY09182). (Lower left) quantitative analysis of γ-H2Av intensity. γ-H2Av intensity was normalized by that of nuclear DAPI (blue). Salivary glands were counterstained by α-tubulin (green). n=20. Error bars are s.d. ***P<0.001. #P>0.02 (t-test). (Lower right) western blot analysis to detect γ-H2Av levels in wild-type and indicated genotypes. Relative band intensities were quantified (bar graphs). Error bars are s.e.m. Performed in triplicate. Scale bar, 40 µm. Fig 7.
PMID: 24352200

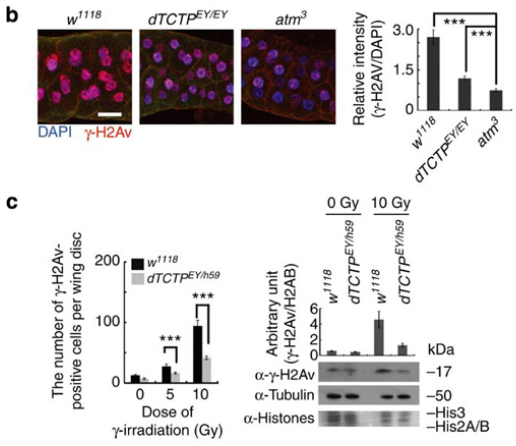

Immunofluorescence Microscopy

(b) Reduced γ-H2Av levels in salivary gland cells from both dTCTPEY/EY and atm3 mutants. Histogram indicates quantitative analysis of γ-H2Av intensity. Error bars are s.e.m. ***P<0.001 (t-test). Performed in triplicate. Scale bar, 40 µm. (c) (Left) γ-H2Av foci formation in IR-exposed wing discs. At 5 and 10 Gy of IR, dTCTPEY/h59 mutants (grey bars) show low levels of γ-H2Av compared with w1118 control (black bars). Third instar larvae treated with different doses of IR were rested for 1 h and dissected. n=9–12. Error bars are s.d. ***P<0.001 (t-test). (Right) western blot analysis in IR-exposed wing discs. Relative band intensities were quantified (bar graphs). Error bars are s.e.m. Performed in triplicate. Fig 7.
PMID: 24352200

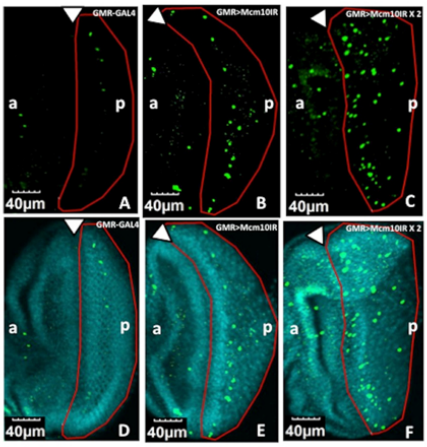

Immunofluorescence Microscopy
The eye imaginal discs were stained with anti-phospho H2AvD antibody (Green) (A, B, C). Also shown are merged images of the eye discs stained with DAPI for DNA (Blue) and anti-phospho H2AvD antibody (Green) (D, E, F). (A, D) GMR-GAL4/yw; +; +; (B, E) GMR-GAL4/yw; +; UAS-Mcm10IR633-700/+; (C, F) GMR-GAL4/yw; +; UAS-Mcm10IR633-700/UAS-Mcm10IR633-700. The white arrowhead shows the morphogenetic furrow. The flies were reared at 28°C. Bars indicate 40 µm. The red border line indicates the posterior region. (a) indicates anterior, (p) indicates posterior. Fig 6.
PMID: 24686397

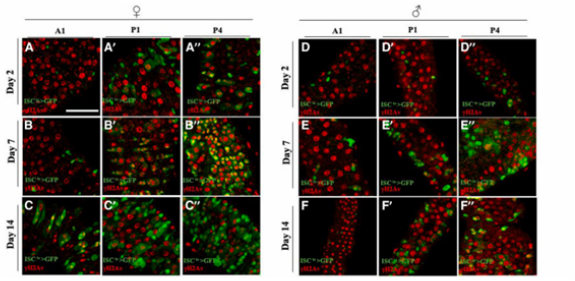

Immunofluorescence Microscopy
(A-F) γH2Av expression in the A1 (A-F), P1 (A'-F') and P4 (A''-F'') regions of 2- (A, D), 7- (B, E) and 14-day-old (C, F) ISCts-GFP females (A-C) and males (D-F). Fig 5.
PMID: 40060901

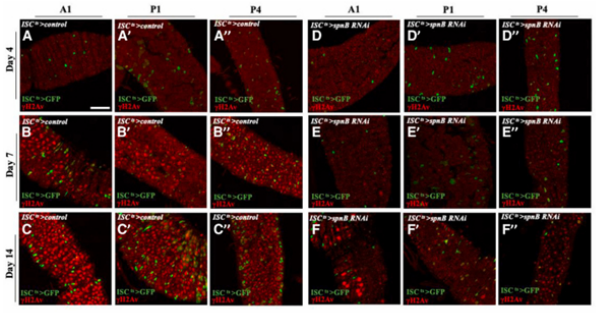

Immunofluorescence Microscopy
(A-F) γH2Av expression in the A1 (A-F), P1 (A'-F') and P4 (A''-F'') regions of young ISCts-Gal4 UAS-GFP (A-C) and ISCts-Gal4 UAS-GFP, UAS-spn-BRNAi (D-F) females induced for 4- (A, D), 7- (B-E) and 14-day (C, F) at 29°C. Fig 6.
PMID: 40060901

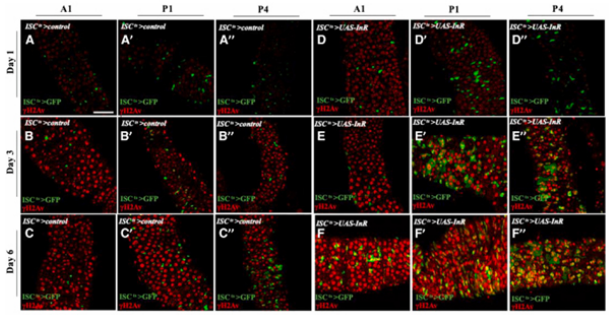

Immunofluorescence Microscopy
(A-F) γH2Av expression in the A1 (A-F), P1 (A'-F') and P4 (A"-F") regions of young ISCts-Gal4 UAS-GFP (A-C) and ISCts-Gal4 UAS-GFP, UAS-InR (D-F) females induced for 1- (A, D), 3- (B-E) and 6-day (C, F) at 29°C. Fig 7. PMID: 40060901

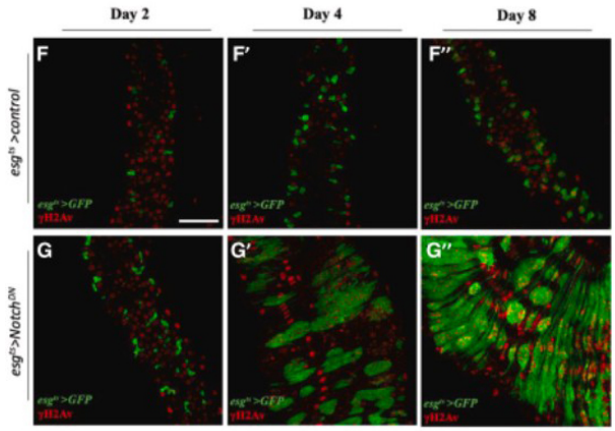

Immunofluorescence Microscopy
(F and G) γH2Av mean pixel intensity per P4 midgut region (red) and ISCs and progenitors (green) of esgts-Gal4 UAS-GFP (F) and esgts-Gal4 UAS-GFP UAS-NotchDN (G) females induced for 2- (F-G), 4- (F'-G') and 8-day (F"-G") at 29°C. Scale bar: 50 µm. Fig 8. PMID: 40060901

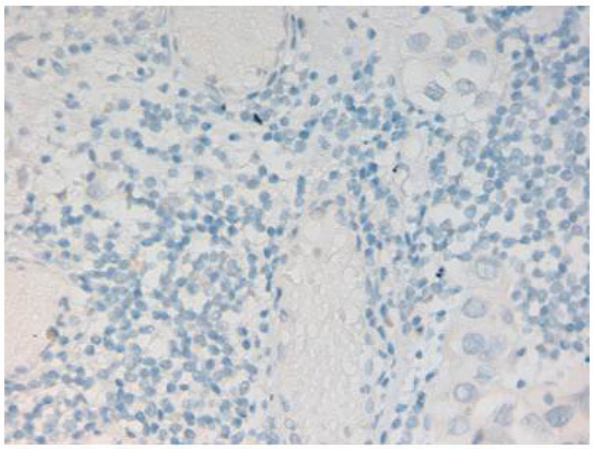

Immunohistochemistry
Immunohistochemistry with anti-Histone Antibody. Tissue: Human Bladder Cancer. Fixation: FFPE buffered formalin 10% conc. Ag Retrieval: HIER citrate buffer pH6 or HIER EDTA pH9. Primary antibody: 2 ug/ml at 2 hr. Secondary Ab: anti rabbit polymer HRP 20 ' RT.

Western Blot
Western blot using Rockland's affinity purified anti-histone H2AvD pS137 antibody shows detection of a band at ~15 kDa corresponding to phosphorylated H2AvD (lane 2 arrow-head). Lane 1: mock-irradiated Drosophila melanogaster (3rd instar) larvae brain WC lysate. Lane 2: 4000-RAD gamma irradiated Drosophila melanogaster (3rd instar) larvae brain WC lysate. Separated on by SDS-PAGE and transferred to nitrocellulose. After blocking the membrane was probed with the primary antibody diluted to 1:500. Washes and reaction with secondary antibody followed incubation. Use HRP conjugated Gt-a-Rabbit IgG [H&L] MX (p/n 611-103-122) and ECL for detection. Personal Communication. Yikang Rong, NIH, CCR, Bethesda, MD.

References

- Neophytou C et al. Aberrant enterocyte progenitor clustering as an early life biomarker of Drosophila aging. *iScience.* (2025)
- Na HJ et al. Integrated ecdysone and O-linked N-acetylglucosamine signaling coordinates intestinal stem cell proliferation in Drosophila midgut. *G3 (Bethesda).* (2025)
- Watase GJ et al. RNA polymerase II-mediated rDNA transcription mediates rDNA copy number expansion in Drosophila. *PLoS Genet.* (2024)
- Pilesi E et al. Vitamin B6 deficiency cooperates with oncogenic Ras to induce malignant tumors in Drosophila. *Cell Death Dis.* (2024)
- Parrella P et al. Bleomycin reduces Vairimorpha (Nosema) ceranae infection in honey bees with some evident host toxicity. *Microbiol Spectr.* (2024)
- Chauvin SD et al. Inherited C-terminal TREX1 variants disrupt homology-directed repair to cause senescence and DNA damage phenotypes in Drosophila, mice, and humans. *Nat Commun.* (2024)
- Rye T et al. Nup153 is not required for anchoring heterochromatic DSBs to the nuclear periphery. *MicroPubl Biol.* (2024)
- Guo T et al. Impaired dNKAP function drives genome instability and tumorigenic growth in Drosophila epithelia. *J Mol Cell Biol.* (2024)
- Crucianelli C et al. Distinct signaling signatures drive compensatory proliferation via S-phase acceleration. *PLoS Genet.* (2023)
- Torre M et al. A Drosophila model relevant to chemotherapy-related cognitive impairment. *Sci Rep.* (2023)
- Chang YH et al. Endogenous retroviruses and TDP-43 proteinopathy form a sustaining feedback driving intercellular spread of Drosophila neurodegeneration. *Nat Commun.* (2023)
- Zhang Q et al. Phase separation of BuGZ regulates gut regeneration and aging through interaction with m6A regulators. *Nat Commun.* (2023)

- Fontana P et al. Serine ADP-ribosylation in Drosophila provides insights into the evolution of reversible ADP-ribosylation signalling. *Nat Commun.* (2023)
- Torre M et al. A Drosophila model relevant to chemotherapy-related cognitive impairment. *Sci Rep.* (2023)
- González-Marín B et al. ATM/Chk2 and ATR/Chk1 Pathways Respond to DNA Damage Induced by Movento® 240SC and Envidor® 240SC Keto-Enol Insecticides in the Germarium of Drosophila melanogaster. *Toxics.* (2023)
- Tu R et al. Gap junction-transported cAMP from the niche controls stem cell progeny differentiation. *Proc Natl Acad Sci U S A.* (2023)
- Munden, A et al. Identification of replication fork-associated proteins in Drosophila embryos and cultured cells using iPOND coupled to quantitative mass spectrometry. *Scientific Reports* (2022)
- Gemble, S et al. Genetic instability from a single S phase after whole-genome duplication. *Nature* (2022)
- Richards L et al. Nucleoporins facilitate ORC loading onto chromatin. *Cell Rep.* (2022)
- O'Neill RS et al. Traip controls mushroom body size by suppressing mitotic defects. *Development* (2022)
- Liu J et al. NMNAT promotes glioma growth through regulating post-translational modifications of P53 to inhibit apoptosis. *Elife.* (2021)
- Lattao R et al. Mauve/LYST limits fusion of lysosome-related organelles and promotes centrosomal recruitment of microtubule nucleating proteins. *Dev Cell.* (2021)
- Casale AM et al. Transposable element activation promotes neurodegeneration in a Drosophila model of Huntington's disease. *iScience* (2021)
- Hatkevich t et al. A pathway for error-free non-homologous end joining of resected meiotic double-strand breaks. *Nucleic Acids Res.* (2021)
- Tu R et al. Multiple Niche Compartments Orchestrate Stepwise Germline Stem Cell Progeny Differentiation. *Curr Biol.* (2021)
- Mascolo E et al. Pyridoxine/pyridoxamine 5'-phosphate oxidase (Sgll/PNPO) is important for DNA integrity and glucose homeostasis maintenance in Drosophila. *J Cell Biol.* (2020)
- Rastegari E et al. WD40 protein Wuho controls germline homeostasis via TRIM-NHL tumor suppressor Mei-p26 in Drosophila. *Development.* (2020)
- Palladino J et al. Targeted de novo centromere formation in Drosophila reveals plasticity and maintenance potential of CENP-A chromatin. *Dev Cell.* (2020)
- Na HJ et al. Nutrient-driven O-GlcNAcylation controls DNA damage repair signaling and stem/progenitor cell homeostasis. *Cell Rep.* (2020)
- Lin KY et al. Piwi reduction in the aged niche eliminates germline stem cells via Toll-GSK3 signaling. *Nat Commun.* (2020)
- Merigliano C et al. A new role for Drosophila Aurora-A in maintaining chromosome integrity. *Chromosoma.* (2019)
- Cosolo A et al. JNK-dependent cell cycle stalling in G2 promotes survival and senescence-like phenotypes in tissue stress. *Elife* (2019)
- Okumura K et al. Genetic identification and characterization of three genes that prevent accumulation of oxidative DNA damage in Drosophila adult tissues. *DNA Repair (Amst).* (2019)

- View More ...

Disclaimer

This product is for research use only and is not intended for therapeutic or diagnostic applications. Please contact a technical service representative for more information. All products of animal origin manufactured by Rockland Immunochemicals are derived from starting materials of North American origin. Collection was performed in United States Department of Agriculture (USDA) inspected facilities and all materials have been inspected and certified to be free of disease and suitable for exportation. All properties listed are typical characteristics and are not specifications. All suggestions and data are offered in good faith but without guarantee as conditions and methods of use of our products are beyond our control. All claims must be made within 30 days following the date of delivery. The prospective user must determine the suitability of our materials before adopting them on a commercial scale. Suggested uses of our products are not recommendations to use our products in violation of any patent or as a license under any patent of Rockland Immunochemicals, Inc. If you require a commercial license to use this material and do not have one, then return this material, unopened to: Rockland Inc., P.O. BOX 5199, Limerick, Pennsylvania, USA.